Geofísica Internacional (2025) **64-4**: 1731- 1750

Permeability estimation using Poiseuille models: a case study on comparative analysis of characteristic radii in tight rocks

Moisés Franco-Villegas[1], Enrique Coconi-Morales[2,*], Carlos J.T. Nieto-Rivero[1], Oscar. C. Valdiviezo-Mijangos[3] and Gorgonio Fuentes-Cruz[3]

Abstract

Permeability, a fundamental petrophysical property controlling fluid flow in porous media, faces measurement challenges in tight rocks due to time-intensive procedures, specialized equipment requirements, and high costs. This study develops a novel Poiseuille-based methodology that systematically identifies optimal characteristic radii from routine mercury injection capillary pressure (MICP) data while revealing the underlying physical mechanisms. Seventeen characteristic pore-throat radii were systematically evaluated from compiled datasets of tight sandstones, carbonates, and shales. Model performance, assessed by coefficient of determination (R^2), yielded 0.96 for sandstones with R_c (critical radius at percolation threshold), 0.86 for carbonates with r_{60}-r_{70} (radii at 60-70% mercury saturation), and 0.77 for shales with r_5-r_{10} (radii at 5-10% saturation). These radii provide physical mechanisms beyond empirical fitting: R_c captures early percolation in preserved intergranular networks, r_{60} to r_{70} represents cumulative saturation needed for smaller throats to bridge isolated vugs and molds in heterogeneous carbonate systems, and r_5 to r_{10} identifies the largest pores controlling nanoscale connectivity despite being least abundant. For tight reservoirs and CO2 storage projects where direct measurements are impractical, this approach enables rapid characterization using collapsed fragments or drilling cuttings when core recovery is limited, reducing evaluation costs through lithology-specific models.

Key words: Permeability, Poiseuille model, Characteristic radius, Percolation, Tight rock.

Resumen

La permeabilidad, una propiedad petrofísica fundamental que controla el flujo de fluidos en medios porosos, enfrenta desafíos de medición en rocas compactas debido a procedimientos intensivos en el tiempo, requisitos de equipos especializados y altos costos asociados. Este estudio presenta una nueva metodología basada en modelos Poiseuille que identifica sistemáticamente los radios característicos de los datos de presión capilar de inyección de mercurio (MICP) a la par que revela los mecanismos físicos subyacentes. Se evaluaron sistemáticamente diecisiete radios característicos de garganta de poro a partir de conjuntos de datos compilados de areniscas, carbonatos y lutitas de baja permeabilidad. El desempeño del modelo, evaluado mediante el coeficiente de determinación (R^2), arrojó 0.96 para areniscas con R_c (radio crítico en el umbral de percolación), 0.86 para carbonatos con r_{60}-r_{70} (radios al 60-70% de saturación de mercurio), y 0.77 para lutitas con r_5-r_{10} (radios al 5-10% de saturación). Estos radios proporcionan mecanismos físicos más allá del ajuste empírico: R_c captura la percolación temprana en redes intergranulares preservadas, r_{60} a r_{70} representa la saturación acumulativa necesaria para que gargantas más pequeñas conecten vúgulos y poros móldicos aislados en sistemas carbonatados heterogéneos, y r_5 a r_{10} identifica los poros más grandes que controlan la conectividad a nanoescala a pesar de ser los menos abundantes. Para yacimientos de baja permeabilidad y proyectos de almacenamiento de CO2 donde las mediciones directas son imprácticas, este enfoque permite la caracterización rápida fragmentos colapsados de núcleos o recortes de perforación cuando la recuperación de núcleos es limitada, reduciendo los costos de evaluación mediante modelos específicos por litología.

Palabras clave: Permeabilidad, Modelo Poiseuille, Radio característico, Percolación, roca compacta.

Received: March 22, 2025; Accepted: August 7, 2025; Published on-line: October 1, 2025.

Editorial responsibility: Dr. Francisco J. Valdés-Parada

* Corresponding author: Enrique Coconi-Morales, ecoconi@imp.mx
[1] Instituto Mexicano del Petróleo, Posgrado, Ciudad de México (CDMX), México.
[2] Instituto Politécnico Nacional, ESIA Unidad Ticomán, Ciudad de México (CDMX), México.
[3] Instituto Mexicano del Petróleo, Dirección de Investigación, Gerencia de Investigación en Explotación, Ciudad de México (CDMX), México.

https://doi.org/10.22201/igeof.2954436xe.2025.64.4.1877

1. Introduction

Tight rocks have emerged as significant hydrocarbon resources capable of extending production for several decades (Boak and Kleinberg, 2020). These formations, characterized by permeability values below 1 mD and porosity less than 12% (Boak and Kleinberg, 2020; Zhang *et al.* (2016)), present unique challenges for reservoir characterization.

Permeability characterization is fundamental to enhanced hydrocarbon recovery, reservoir simulation, and CO2 storage applications (Mohaghegh *et al.*, 1995; Salazar and Villa, 2007; Ozota *et al.*, 2021). The permeability can be estimated with permeameters in core samples or well testing. However, the information from both techniques is limited due to their associated costs (Mohaghegh *et al.*, 1995; Rezaee, 2006). Analytical permeability models have emerged as pragmatic tools for estimation when direct measurements are unavailable. While permeability constitutes a second-rank symmetric tensor reflecting the anisotropic nature of porous media (Bear, 2018), practical models typically express it as a scalar function of two components: a connectivity term that accounts for the microstructural arrangement of the pore network, and a characteristic length scale corresponding to the pore-throat radius (Bernabé et al., 2010; Pittman, 1992). Mercury injection capillary pressure (MICP) analysis characterizes pore-throat size distributions in tight rocks (Giesche, 2006). This technique has proven equally effective when applied to drilling cuttings or collapsed fragments, yielding pore-throat size distributions comparable to those obtained from intact core samples (Swanson, 1981; Rezaee *et al.*, 2006). Consequently, drilling cuttings from intervals where core recovery is limited or economically unfeasible can be analyzed through MICP to derive characteristic radii for permeability estimation.

The semi-empirical Poiseuille approach provides a framework for permeability estimation, wherein the connectivity parameter is proportional to porosity and the characteristic length corresponds to a single pore-throat radius representative of the pore network. Despite this apparent simplicity, selecting the appropriate characteristic radius from MICP data presents a fundamental challenge that has generated diverse approaches in literature. Two distinct methodologies have emerged for radius selection. The first employs percolation theory to identify physically meaningful radii. Katz and Thompson (1986, 1987) introduced the critical radius (R_C), corresponding to the inflection point where mercury establishes continuous pathways through the pore network. Pittman (1992) refined this approach with the apex radius (R_{apex}), which identifies percolation through saturation pressure ratio analysis, proving particularly effective for rocks with well-defined modal pore distributions. Alternatively, Dastidar *et al.*, (2007) developed a statistical approach using the weighted geometric mean radius (R_{WGM}), which accounts for the entire pore-throat spectrum by weighting each radius by its saturation increment. This method addresses limitations in tight rocks where no single percolation threshold dominates flow behavior.

The second methodology relies on empirical correlations using percentile-based radii. Various percentile levels (r_{10}, r_{25}, r_{35}, r_{50}, etc) have been employed with markedly inconsistent performance across lithologies (Kolodzie, 1980; Pittman, 1992; Rezaee *et al.*, 2006; Rezaee *et al.*, 2012; Ngo *et al.*, 2018; Liu *et al.*, 2020; Vafaie *et al.*, 2021). These empirical approaches typically lack physical justification. The absence of physical interpretation proves problematic for rocks exhibiting minimal porosity sensitivity while showing strong dependence on specific pore-throat radii, as demonstrated by the r_{50} model (Gao and Hu (2013).

The challenge of permeability estimation in tight rocks is addressed by systematically identifying which characteristic pore-throat radius from MICP data best predicts permeability for each lithology. Physical connections between specific radii and percolation mechanisms controlling flow in different rock types are established, unlike previous empirical approaches. Seventeen characteristic radii were evaluated across compiled datasets of tight sandstones, carbonates, and shales, including three theory-based radii (R_C, R_{apex}, R_{WGM}) and fourteen percentile radii (r_5 to r_{70}). Distinct lithology-specific responses were revealed through coefficient of determination assessment: $R^2 = 0.96$ was achieved for sandstones with Rc (critical radius at percolation threshold), $R^2 = 0.86$ for carbonates with r_{60}-r_{70} (60-70% mercury saturation), and $R^2 = 0.77$ for shales with r_5-r_{10} (5-10% saturation), with conventional models being significantly outperformed.

This work presents a novel methodology that employs Poiseuille models as interpretive tools revealing why specific pore-throat radii control permeability: early percolation in preserved intergranular networks is captured for tight sandstones, cumulative saturation requirements to bridge isolated vugs and moldic pores are represented for carbonates, and nanoscale connectivity controlled by the largest, yet least abundant pores is identified for shales. Cost-effective permeability estimation is enabled for tight reservoirs and CO2 storage projects where direct measurements are impractical, with lithology-specific solutions being applicable to both cores and drilling cuttings.

The manuscript is organized as follows: Section 2 establishes the theoretical framework, presenting MICP fundamentals, percolation concepts, and descriptions of the analyzed tight rock datasets. Section 3 presents comprehensive results examining permeability-radius relationships across lithologies, evaluates the predictive performance of different characteristic radii, and explores the relationships between sedimentary environments

and percolation behavior. Section 4 synthesizes these findings to discuss their physical significance and practical implications for permeability estimation in tight formations. The conclusions summarize the key contributions.

2. Methods and materials

2.1. Theoretical background of MICP

The MICP curve represents the increasing saturation of mercury as a function of pressure (Rezaee *et al.*, 2012). During the MICP test, the pressure increases to overcome the capillary pressure of the pore-throats. The mercury enters the pore network omnidirectionally, initiating invasion percolation or drainage.

MICP curves exhibit distinct morphologies that reflect the PTSD of the sample's pore network (Rezaee *et al.*, 2006). These morphological characteristics are also influenced by the topological properties of the pore network, e.g., pore accessibility and connectivity (Zhao *et al.*, 2023).

The shape of the throats can be conceptualized as cylinders, a simplification that enabled Washburn (1921) to propose a relation between capillary pressure and pore-throat radius:

$$r = -\frac{2\gamma cos\theta}{P_c}, \tag{1}$$

where P_C is the capillary pressure (MPa), r is the capillary radius (m), γ is the Surface tension (0.485N/m), and θ is the contact angle of mercury (140°). These standard values for mercury-air systems are widely adopted in petroleum research (Webb, 2001; Giesche, 2006; Rezaee *et al.*, 2006; Comisky *et al.*, 2007), enabling consistent comparison across studies. However, the calculated pore-throat radius depends on the specific fluid system used (Hildenbrand *et al.*, 2002; Huet *et al.*, 2005; Amann-Hildenbrand *et al.*, 2013). Furthermore, porous media can exhibit multiple contact angles, with significant variations occurring even within the same sample due to intra-sample mineralogical heterogeneity (León y León, 1998; Amann-Hildenbrand *et al.*, 2013). Additionally, variations in contact angle and surface tension can occur for pores with radii smaller than 5 nm, where relative errors as high as 44% have been reported (Wang *et al.*, 2016).

From the pore-throat sizes the PTSD is derived, in this work, the differential saturation versus log pore-throat radius ($ds/dlog(r)$) format was employed due to their capacity to embolden larger pore-throat ranges (Liu and Ostadhassan, 2019). This range of sizes is prone to contribute more to permeability.

2.2. Classification of pores based on the percolation function

Hildenbrand *et al.*, (2002) and Yokoyama and Takeuchi (2009) proposed classifying pores as a function of their contribution to the fluid flows (percolation function). This classification helps quantify the fraction of the pore network that contributes to flow, as the definitions of some researchers may differ. The total porosity is the quantification of the total volume of pores connected or isolated, connected pores these pores and throats forms the pore network that connect the external faces of the porous medium in this case the tight rocks, isolated pores serve more as a potential storage capacity but do not contribute to the percolation, transport porosity (ϕ_t) is the fraction of the pore network that contributes effectively to the percolation also known as backbone fraction (Sahimi, 2021), dead end pores that are connected to the pore network but do not contribute to the percolation. Figure 1 schematically illustrates this classification based on the percolation function.

During the MICP test, various researchers proposed criteria to identify the moment when the mercury saturation reaches the threshold necessary for the transport fraction of the pore network to percolate. This critical point is significant because the corresponding pressure can be applied in equation (1) to derive a characteristic radius representing the pore network's transport fraction.

Katz and Thompson (1986, 1987) proposed the inflection point of the MICP curve to identify the moment when the percolation begins. This point can be determined by calculating the first derivative of saturation to log radius ($ds/dlog(r)$), where the maximum value of this derivative corresponds to the inflection point of the original curve (Amann-Hildenbrand et al., 2013). However, it can be challenging to determine, even without showing a threshold pressure inflection point (Pittman, 1992; Zhao *et al.*, 2023).

On the other hand, Pittman proposed a graphical method to detect this threshold pressure, which involves plotting the mercury saturation divided by capillary pressure on the y-axis and the mercury saturation on the x-axis. The plot shows an apex corresponding to the pressure threshold and saturation level, forming continuous flow paths through the pore network. However, this method is helpful for lithologies that have a remarkable mode in their PTSD.

Figure 2 illustrates the application of Pittman's method to two contrasting rock types. In Figure 2a, a carbonate sample displays a well-defined apex at 47.4% saturation, indicating a dominant pore-throat system. Conversely, Figure 2b shows a shale sample where the S/P ratio decreases monotonically without exhibiting a discernible apex, reflecting the absence of a dominant interconnected pore network.

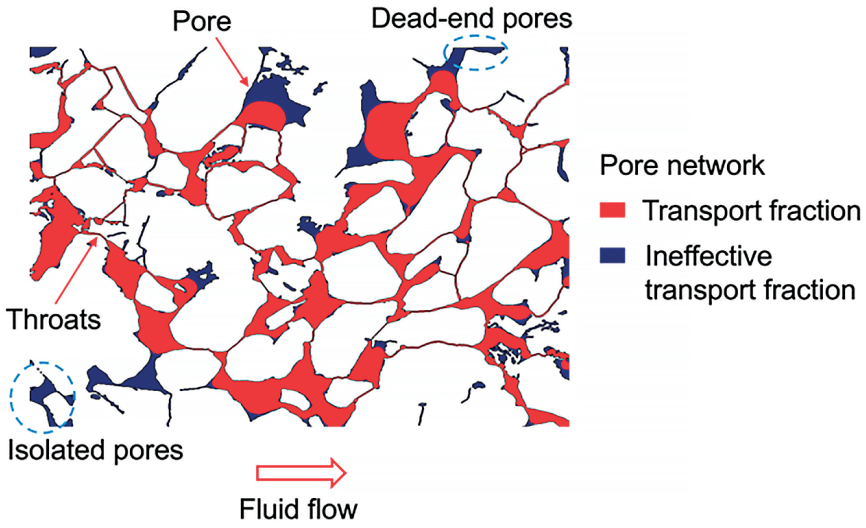

Figure 1. A pore network cross-section represents the percolation function of each pore

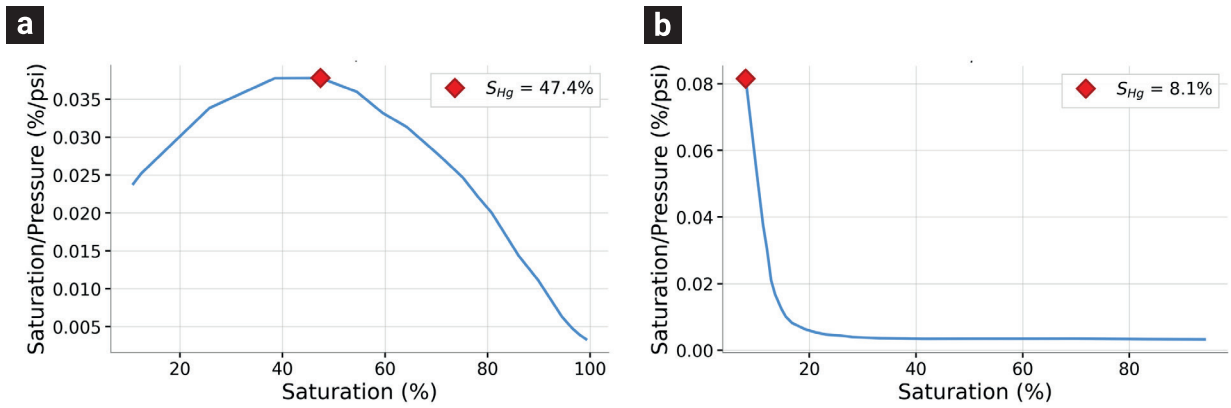

Figure 2. Pittman's method plots saturation/pressure ratio versus mercury saturation. (a) Carbonate sample with clear apex at 47.4% saturation, marking the percolation threshold. (b) Shale sample showing monotonic decrease without apex definition at 8.1% saturation.

From the saturation associated with the percolation threshold, the transport porosity can be quantified as:

$$\phi_t = \phi S_{\%}, \tag{2}$$

where $S_{\%}$ represents the saturation at the percolation threshold (via apex or inflection point). This value provides an approximation of the effective porosity, as dead-end pores become saturated but do not contribute to the continuous mercury flow paths.

An alternative to percolation-based approaches is the weighted geometric mean radius (R_{WGM}) proposed by Dastidar *et al.*, (2007). This radius includes the entire spectrum of the pore-throats. It represents a statistically characteristic length that captures the contribution of the entire pore-throat size distribution to fluid flow. They noted the contribution of this parameter in tight lithologies, where the pore-throat sizes are dimensionally similar, including the contribution of the smaller pore-throats, as follows:

$$R_{wgm} = \left(\prod_{i=1}^{n} R_i^{w_i}\right)^{1/\sum_{i=1}^{n} w_i}, \tag{3}$$

$$w_i = \frac{a_i}{a_T}, \tag{4}$$

where R_i is the i-th pore-throat radii (μm), w_i is the corresponding contribution weight ($adim$), a_i is the incremental saturation (a_T), and a_T is the total incremental saturation (%).

2.3. Poiseuille models

2.3.1 Semi-empirical model development

The assumption about Poiseuille models is that porous media (such as rocks) can be conceptualized as a bundle of capillaries, the permeability is modeled as a function of the porosity (ϕ) and a characteristic radius (r).

For N parallel capillaries, Hagen-Poiseuille gives $Q=(N\pi r^4\Delta P)/(8\mu L)$, while Darcy's law gives $Q=(kA\Delta P)/(\mu L)$. Equating these and substituting porosity $\phi=N\pi r^2/A$ yields:

$$k = c\phi r^2, \tag{5}$$

where c is a constant associated with the pore geometry (Hunt, 2001).

However, real pore networks are not idealized capillaries. They exhibit tortuosity, variable pore sizes, irregular geometries, and complex connectivity. To account for these particularities, preserving the functional form of equation (5), researchers generalized it as a semi-empirical expression:

$$k = c\phi^m r^n, \tag{6}$$

where m and n are empirical fitting parameters that capture the effects of pore network complexity. For regression analysis, this relationship is commonly expressed in logarithmic form (see Table 1 for various implementations):

$$Ln(k/k_0) = \ln(c) + mLn(\phi) + nLn(r/r_0). \tag{7}$$

Where $k_0 = 1mD$ and $r_0 = 1\mu m$ are reference values to maintain dimensional consistency. In practice, k is expressed in mD, ϕ as a fraction, and r in μm, with logarithms applied to these numerical values a standard approach in petroleum engineering correlations (Kolodzie, 1980; Pittman, 1992; Rezaee *et al.*, 2006).

These models have two fundamental limitations: they assume idealized pore geometries and predict only scalar permeability. While permeability is a directional property (second-order tensor), MICP's omnidirectional mercury invasion captures only bulk pore-throat distribution without any directional information.

Despite these limitations, Poiseuille-based models serve specific purposes in reservoir characterization. They are valuable for rapid permeability screening when MICP represents the only feasible measurement, such as with drill cuttings or damaged core samples unsuitable for a conventional permeameter. In relatively isotropic formations, the scalar approximation provides reasonable estimates for flow capacity assessment.

2.3.2 Literature models

Based on the semi-empirical framework presented above, numerous researchers have developed specific correlations for different rock types. Table 1 summarizes these models, highlighting the diversity of characteristic radius associated with a level of saturation.

Kolodzie (1980) presents the Windland equation, which states that, given a certain porosity, larger throats in the pores will result in greater flow through and permeability. Kolodzie (1980) slightly modified this equation for the calculation of the pore-throat size. Pittman (1992) developed empirical equations for calculating the radii, both uncorrected for air permeability. Dastidar *et al.*, (2007) established an empirical relationship linking Klinkenberg's corrected permeability, porosity, and R_{WGM}. They also developed a correlation involving Klinkenberg's corrected permeability, porosity, and the pore radius at 35% mercury saturation (r_{35}). Rezaee *et al.*, (2006) developed empirical equations to calculate permeability based on porosity and pore-throat radii at various mercury saturation percentiles, with the r_{50} case showing the highest correlation coefficient for carbonates with complex pore networks. Rezaee *et al.* (2012) also developed empirical equations linking permeability to pore-throat sizes, based on mercury injection analysis and nuclear magnetic resonance data, with the pore-throat radius r_{10} being the most accurate predictor of permeability for tight gas sands. Ngo *et al.* (2018) established various empirical relationships between permeability, porosity, and pore-throat size with mercury saturation, emphasizing the most accurate cases for sandstones and carbonates. Vafaie *et al.* (2021) conducted multiple linear regression analyses involving permeability, porosity, and pore-throat radii, where the optimal fit was achieved using the pore-throat radius r_{55} , corresponding to a mercury saturation of 55%.

The variety of characteristic radii across these studies highlights an important point: no single radius can universally predict permeability for all rock types. This research on finding the best characteristic radius for different tight rock categories is driven by this observed diversity.

2.4. Tight rocks

Hydrocarbon storage in tight rocks can extend production for at least three decades (Boak and Kleinberg, 2020). In this sense, the permeability of these rocks controls production. The rate of hydrocarbons is also relevant for operations like CO2 storage, where the gas breakthrough pressure (P_{bt}), which is the minimum pressure required for the gas to penetrate the seal rock, follows an inverse proportional relationship with permeability ($P_{bt} \propto k^{-0.45}$). Interested readers are encouraged to consult the work of Fleury

Table 1. List of several models that relate permeability, porosity, and radii through Poiseuille models.

Model	Characteristics	Author
Winland Equation $0.588\log(k)=-0.732+0.864\log(\phi)+\log(r_{35})$ Kolodzie Equation (Modified Windland Equation) $0.5547\log(k)=-0.9058+0.9033\log(\phi)+\log(r_{35})$	Lithology Sandstones	Kolodzie (1980)
$\log(k)=-0.861+1.185\log(\phi)+1.627\log(R_{apex})$ $R^2=0.928$ $\log(k)=-1.221+1.415\log(\phi)+1.512\log(r_{25})$ $R^2=0.939$	Lithology Sandstones No. Samples 202	Pittman (1992)
$\log(k)=-1.16+1.78\log(\phi)+0.93\log(r_{50})$ $R^2=0.787$	Lithology Carbonates No. Samples 144	Rezaee *et al.* (2006)
$\log(k)=-2.51+3.06\log(\phi)+1.64\log(R_{WGM})$ $\log(k)=-3.03+3.06\log(\phi)+1.35\log(r_{35})$	Lithology Tight sands No. Samples 150	Dastidar *et al.* (2007)
$\log(k)=-1.92+0.949\log(\phi)+2.18\log(r_{10})$ $R^2=0.781$	Lithology Tight gas sands No. Samples 16	Rezaee *et al.* (2012)
Sandstones $\log(k)=-7.949+8.948\log(\phi)-0.382\log(r_{55})$ $R^2=0.965$ Carbonates $\log(k)=-2.039+1.936\log(\phi)+1.226\log(r_{20})$ $R^2=0.849$	Lithology Sandstones and carbonates	Ngo *et al.* (2018)
$\log(k)=-1.88+0.99\log(\phi)-0.12\log(r_{55})$ $R^2=0.76$	Lithology Tight gas shales No. Samples 12	Vafaie *et al.* (2021)

and Brosse (2018), which addresses more technical aspects of CO2 operations in tight rocks.

In this work, MICP curves from three different tight rocks were digitized: 8 carbonates (Ca), 10 Tight sandstones (Ts), and 7 Shales (Sh). The carbonates and shales were obtained from Liu *et al.*, (2020), while the tight sandstones were from Wang *et al.*, (2019). To validate the accuracy of the digitalization process, the estimated r_{50} values for tight sandstone were compared with the published yielding an average percentage error of 1.52%, which is considered acceptable.

The MICP data analyzed in this study represent three distinct tight rock types from prolific hydrocarbon-bearing formations worldwide. The carbonate samples, provided by Liu *et al.* (2020), originate from the Asmari Formation, a major oil-producing layer in southwestern Iran whose mineralogical composition is dominated by dolomite and anhydrite. These carbonates present a complex porous system characterized by diverse pore types including moldic pores, isolated vuggy pores, intercrystalline pores, and intraparticular pores, with permeabilities ranging from 0.166 to 8.375 mD and porosities from 8.42% to 27.2%. The tight sandstone samples come from the Yanchang Formation in the Ordos Basin, a region renowned for its rich hydrocarbon resources (Yang and Deng, 2013), where these compact rocks exhibit permeabilities ranging from 0.011 to 10.530 mD (average 1.284 mD) and porosities between 8.92% and 17.38% (average 12.86%), with some samples displaying bimodal PTSD patterns (Wang *et al.*, 2019). The shale samples originate from the Songliao Basin, one of the world's richest hydrocarbon basins (Feng and Graham, 2024), and with permeability values ranging from 0.001 to 0.313 mD and correspondingly low porosities between 1.676% and 5.828% (Liu *et al.*, 2020). This diverse sample suite provides a range of tight rock types with varying pore network characteristics.

Table 2 lists the permeability and porosity of the samples used in this study. Although some samples cannot be classified as tight, studying their PTSD helps estimate the saturation where the samples begin to percolate. The tight rocks are from

Table 2. The petrophysical properties of the rock samples.

Sample	Porosity (%)	Permeability (mD)
Ca1	16.31	0.384
Ca2	10.76	0.166
Ca3	13.83	1.121
Ca4	8.74	0.343
Ca5	8.42	0.343
Ca6	17.04	2.298
Ca7	9.89	3.023
Ca10	27.2	7.196
Sh1	1.676	0.001
Sh2	4.152	0.005
Sh3	3.782	0.064
Sh4	5.828	0.313
Sh5	4.486	0.3
Sh6	5.27	0.009
Sh7	4.328	0.008
Ts3	12.58	0.467
Ts4	11.15	0.229
Ts9	11.36	0.112
Ts10	11.31	2.22
Ts16	14.16	3.14
Ts11	13.86	2.29
Ts21	12.83	0.104
Ts22	11.03	0.104
Ts23	11.97	0.011
Ts25	16	10.53

different locations. More details about these samples are in the following sections.

2.5. Performance metrics

To evaluate the predictive performance of the permeability models (radii and Poiseuille regressions), three complementary performance metrics were employed, all computed in logarithmic space to account for the log-distribution of permeability data. The coefficient of determination (R^2) quantifies the proportion of variance in measured permeability values explained by the predictive models through equation (8):

$$R^2 = 1 - \frac{\sum_{i=1}^{n}(y_i - \hat{y}_i)^2}{\sum_{i=1}^{n}(y_i - \bar{y})^2}, \tag{8}$$

where y_i correspond to observed (measured) permeability values, $\hat{y}_i$ the predicted (estimated) permeability values and $\bar{y}$ is the mean of the observed values.

The root mean square error (RMSE) measures the average magnitude of prediction errors in logarithmic space using:

$$RMSE = \sqrt{\frac{\sum_{i=1}^{n}(\hat{y}_i - y_i)^2}{n}}, \tag{9}$$

where n is the number of samples in each rock group. To account for model complexity and provide uncertainty bounds for predictions, the standard error (SE) of regression residuals was calculated as:

$$SE = \sqrt{\frac{\sum_{i=1}^{n}(\hat{y}_i - y_i)^2}{(n - p - 1)}}, \tag{10}$$

where p represents the number of predictor variables in each model ($p = 1$ for single-parameter models using only characteristic radius, and $p = 2$ for models incorporating both radius and porosity). The SE values were subsequently used to construct

error bars for permeability predictions, with these error bars appearing asymmetric when displayed in linear permeability space due to the logarithmic transformation.

2.6. Methodology

The distinctive aspect of this methodology is the integration of permeability-radius space analysis, which is essential for identifying the most representative pore-throat radius characteristic of each tight rock's unique pore network. Conventional approaches typically employ multiple linear regression techniques (e.g., Ngo *et al.*, 2015; Vafaie *et al.* 2021), which often fail to provide a physical interpretation of the selected pore radii. As Noorudin *et al.* (2013) noted regarding the Winland equation, r_{35} showed the best correlation with permeability but without any explanation for this finding. This limitation is particularly significant when analyzing pore networks that exhibit minimal sensitivity to porosity yet demonstrate sensitivity to specific pore-throat radius, as exemplified by the model deduced by Gao and Hu (2013) which incorporates r_{50} as an independent variable, presumably because this radius efficiently captures permeability variance. Recognizing that each tight rock exhibits a specific saturation level required to induce percolation, the proposed methodology aims to identify the most appropriate radius that reflects the percolation threshold for each tight rock type, rather than providing generalized correlations. Under this approach, the saturation level at which each tight rock demonstrates significant sensitivity serves as a reference parameter for rocks with similar pore network characteristics.

Figure 3 illustrates the methodological approach for developing a Poiseuille-based model that identifies the radius reflecting percolation threshold saturation in tight rock pore networks. The process begins with the acquisition of MICP data. For this study, the data are assumed to have been adequately corrected for known artifacts and experimental biases, as detailed in Comisky *et al.* (2007). The second phase involves processing the MICP data, where 17 different characteristic radii were evaluated for all samples (R_C, R_{WGM} and R_{apex}) and 14 percentile-based radii (r_5 to r_{70} in 5% increments) to determine the optimal pore-throat radius. Additionally, the transport porosity corresponding to critical and apex radii (ϕ_t and $\phi_{t,apex}$, respectively) was estimated for evaluation in regression models. Subsequently, a permeability-radius analysis is conducted by conducting a regression analysis between the measured permeability and each characteristic radius, which identifies the radius that most effectively captures the variance in permeability across the sample set of each tight rock type. Following this identification, a multilinear regression analysis incorporating porosity, transport porosity, and the most representative characteristic radius is developed, with model performance evaluated using Equations 8 and 9 to validate predictive capability. The final phase involves a comprehensive discussion of the results, providing a physical interpretation of the relationships between the identified critical radius and permeability behavior in tight rocks.

The following section presents the results and discussion of the tight rock samples analyzed in this work.

3. Results and discussion

3.1. Petrophysical analysis

Tight rocks can show similar porosity and permeability values despite having MICP curve shapes and PTSD. This different response to mercury injection gives important insights into the unique pore network structure of each tight rock type. Figure 4 shows the MICP curves for tight sandstones, carbonates, and shales. To emphasize the heterogeneity, which exists even within similar lithologies, two representative samples from each rock type are shown, along with a comparison of additional samples from the same lithological categories. These comparisons reveal significant differences in pore network traits that are found not only between different rock types but also within rocks of the same category.

3.1.1 Tight Sandstones

Figures 4a and 4b show two tight sandstone samples, both displaying bimodal PTSD. Sample Ts16 has its first mode in the micrometer range, while Ts22's first mode is in the hundreds of nanometers. This difference is important because their permeability values are significantly different: 3.14 mD and 0.104 mD, respectively.

Figure 4c shows a comparison between samples Ts9 and Ts10. Ts10 needs less pressure to start the percolation invasion process, while Ts9 requires higher pressure for invasion to begin. The PTSD indicates that Ts10's first mode appears in the tens of micrometers, whereas Ts9's PTSD is in the hundreds of nanometers, needing more pressure to access these smaller pore-throats.

Notably, tight sandstones with primary modes in the micrometer range show higher permeability values. In contrast, R_{apex} samples with modes in the hundreds of nanometers range have significantly lower permeability. These finer pore networks consistently require higher injection pressures for mercury intrusion and percolation, emphasizing the link between pore-throat sizes and permeability in tight sandstone formations.

The analysis of characteristic radii in the tight sandstone samples is visually coincident with the maximum of the dominant

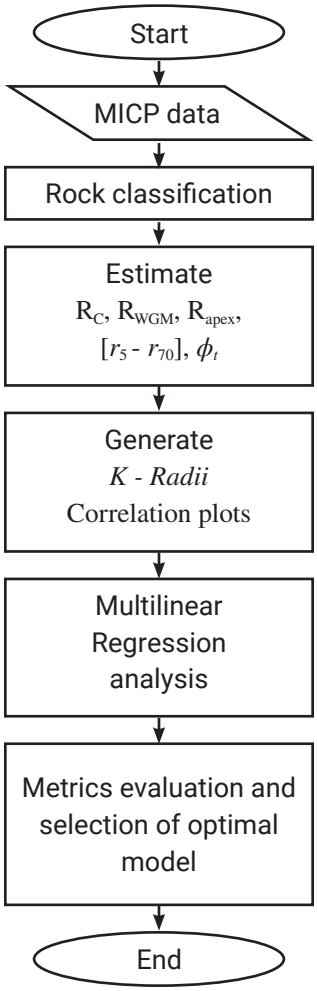

Figure 3. Methodology for developing a Poiseuille-based model using the radius that reflects the percolation threshold saturation in tight rock pore networks.

mode in the PTSD. In contrast, R_{apex}, while consistently located within the modal distribution, does not precisely align with the apex position. Instead, R_{apex} may be situated either before or after the apex, depending on the specific sample characteristics. R_{WGM} exhibits a considerably higher average saturation of 46% and demonstrates variable positioning within the distribution, typically falling between 40th and 60th percentiles in these samples. The R_C in tight sandstone samples visually coincident with the maximum of the dominant mode in the PTSD while R_{apex}, though consistently located within the modal distribution, does not precisely align with the apex position and may be situated either before or after the apex depending on specific sample characteristics. Although precise statistical determination of modal values was not performed, these observations regarding both the relative positioning of characteristic radii within the PTSD and their corresponding saturation levels provide valuable insights into which pore-throat radius populations potentially govern permeability in tight sandstone rocks. The consistent proximity of R_C to the modal maximum, combined with the variable positioning of R_{apex} and R_{WGM} relative to this peak, reflects the method to estimate these characteristics radius.

3.1.2 Carbonates

The carbonate samples exhibit diverse PTSD patterns that reflect their heterogeneous pore networks and distinct characteristic radius positioning compared to tight sandstones. Figures 4d and 4e display two distinctive carbonate samples: Ca3 exhibits a unimodal PTSD with its primary mode in the hundreds of nanometers range followed by a characteristic plateau indicating relatively uniform quantities of various pore-throat sizes before gradually decreasing at dimensions below tens of nanometers, while Ca6 presents a singular, well-defined mode without a plateau, instead showing a continuous decrease that reflects the diminishing presence of pore-throats in the tens of nanometers range. This diversity is further illustrated in Figure 4f, where

samples Ca1 and Ca10, despite their significantly different permeability values of 0.384 mD and 7.196 mD, respectively, display contrasting PTSD patterns. Sample Ca10, with its higher porosity of 17% shows a prominent, well-defined mode followed by continuous decrease, while Ca1 exhibits a mode followed by a plateau similar to Ca3. Unlike tight sandstones, the positioning of R_C in carbonates displays different patterns: R_{apex} typically appears after the maximum value of the mode (observed in 6 out of 8 samples), while R_C consistently manifests before the modal maximum in 7 of the 8 carbonate samples examined, with Ca4 being the single exception where R_C precisely coincides with the PTSD mode maximum. These positional patterns suggest that the complex pore network influences the relationship between characteristic radius and modal features differently than in tight sandstones, potentially reflecting differences in pore connectivity and flow dynamics between these rock types, with R_{WGM} positioned between the P40 and P60 at an average saturation of 53%.

3.1.3 Shales

The shale samples present unique challenges for conventional characteristic radius determination, with both methodological limitations and physical constraints affecting their analysis. The conventional methods for determining R_C and R_{apex} prove inadequate for capturing the representative radius in shale samples because in these extremely tight formations, the inflection point associated with R_C occurs at significantly higher saturations, while R_{apex} is observed at notably lower saturations, and the magnitude of both characteristic radii is highly dependent on the saturation threshold selected for their calculation. Due to these methodological constraints, only R_{WGM} was calculated for the shale samples, yielding an average saturation of 27.4%. Of the seven shale samples analyzed, only two exhibit a slight decrease in the PTSD curve potentially associated with a modal distribution on the nanometer scale, while the PTSD curves for the remaining samples are truncated due to the physical limitation of mercury to access pore-throats smaller than 2.8 nanometers (Sun *et al.*, 2020), preventing complete characterization of the pore network in these ultra-tight formations.

3.1.4 Sedimentological controls on percolation pressure

On the other hand, from Figures 4c, 4f, and 4i, similar lithologies present different percolation thresholds. This reflects the complex interplay between depositional environments and subsequent pore network evolution due to post-depositional modifications. As Pickup *et al.* (1994) demonstrated, permeability variations arise from depositional conditions and subsequent changes through burial, diagenesis, and fracturing, with sedimentary features such as ripples and crossbedding creating heterogeneity across multiple scales.

For the tight sandstones from the Yanchang Formation, the samples potentially represent different facies within the lacustrine turbidite system, including sandy debris flows and interbedded turbidites (Qin *et al.*, 2021; Er *et al.*, 2016). These depositional processes create significant heterogeneity in grain sorting, packing density, and clay content, which directly influence pore-throat connectivity and percolation thresholds. In such lacustrine turbidite environments, various pore types can develop depending on the specific depositional facies and subsequent diagenetic history. Primary intergranular pores typically form between framework grains, while clay mineral aggregates can create their pore networks. Post-depositional processes such as mechanical compaction, authigenic mineral precipitation, and dissolution can significantly modify these primary pore systems (Er *et al.*, 2016).

The Asmari Formation represents deposition in a tropical-subtropical carbonate ramp system with three main environments: inner ramp (restricted and open lagoon, tidal flat), middle ramp, and outer ramp (Seyrafian *et al.*, 2011; Vaziri-Moghaddam *et al.*, 2006). This variability of depositional subenvironments creates significant heterogeneity in petrophysical properties that control pore-throat connectivity. Studies within the Asmari Formation have demonstrated that reservoir quality can vary significantly across different hydraulic flow units, ranging from non-reservoir to good reservoir zones depending on the interplay between depositional facies and diagenetic overprint (Sadeqi *et al.*, 2025). Within the Asmari Formation, inner ramp environments have been documented to develop microporosity, moldic, and vuggy pores, while middle-outer ramp zones exhibit primarily microporosity (Sadeqi *et al.*, 2025). Post-depositional diagenetic processes, including multiphase dolomitization, selective dissolution, and anhydrite cementation, can substantially modify the original pore network (Aqrawi *et al.*, 2006; Al-Aasm *et al.*, 2009).

The shale samples from the Songliao Basin were deposited in a stratified lacustrine system with varying degrees of bottom water anoxia and salinity stratification (Hu *et al.*, 2021), resulting in different lamination patterns and organic matter distribution that influence pore network connectivity. Studies on organic-rich shales within the Songliao Basin have shown that pore connectivity can be significantly affected by heterogeneous organic matter distribution and potential pore occlusion by secondary organic compounds (Zhang et al., 2021). In similar lacustrine shale systems, microphotography analyses have revealed that visible nano porosity can be highly limited, with pore geometries showing progressive modification during burial as indicated by depth-related changes in pore aspect ratios (Zhang et al., 2021). These findings suggest that the complex interactions between

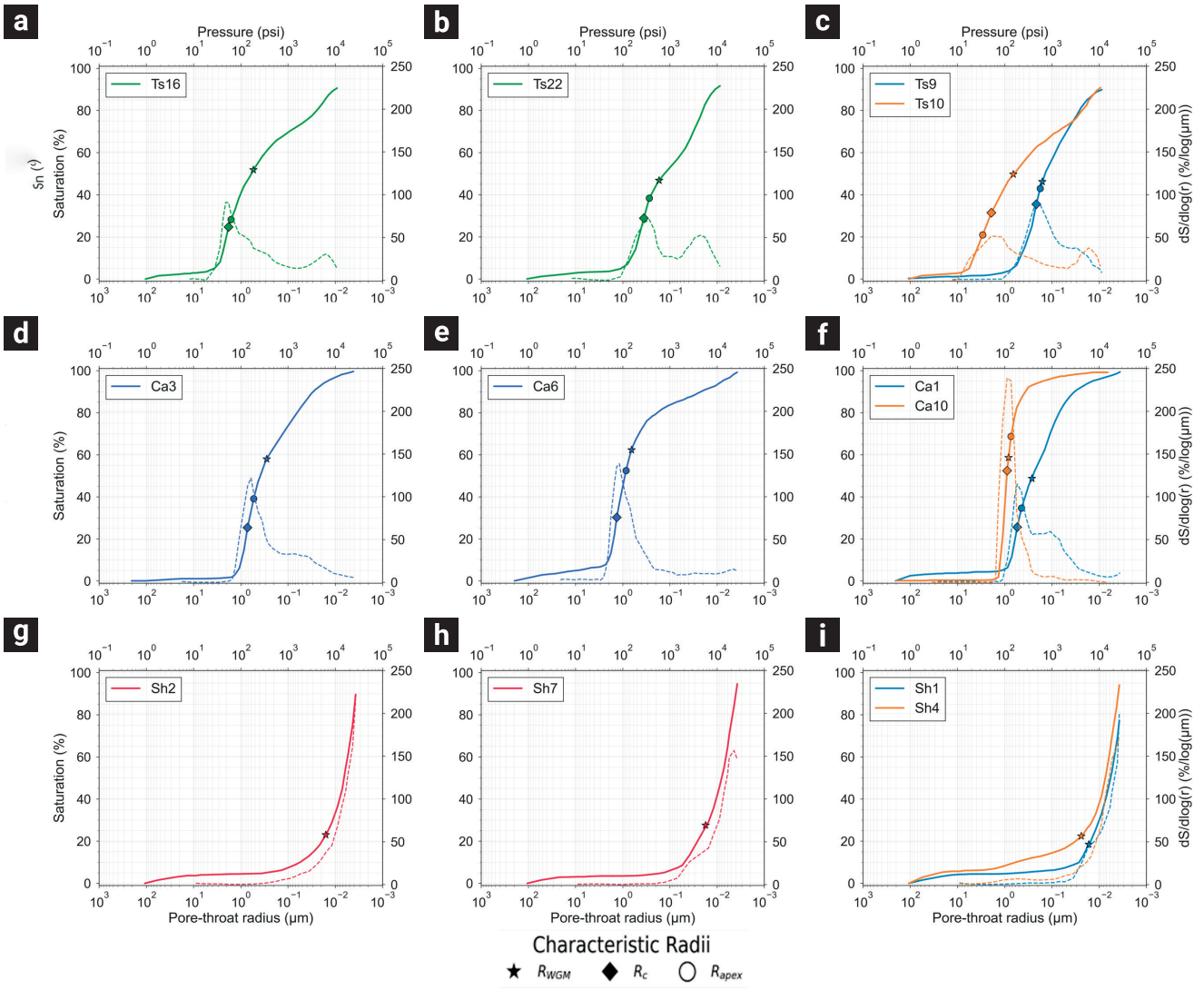

Figure 4. MICP curves display saturation profiles (solid lines) and PTSD (dashed lines) for different tight rocks. a) Sample Ts16; b) Sample Ts22; c) Comparative analysis of samples Ts9 and Ts10; d) Sample Ca3; e) Sample Ca6; f) Comparative chart of samples Ca1 and Ca10; g) Sample Sh2; h) Sample Sh7; i) Comparative analysis of samples Sh1 and Sh4. The differences in PSTD emphasize the pore network characteristics that differentiate tight rocks despite potentially similar porosity and permeability measurements.

primary depositional fabric, organic matter type and distribution, and burial-related processes may similarly influence the heterogeneity in pore-throat connectivity observed in the percolation pressure measurements of the studied samples.

However, the lack of specific sedimentological context in the compiled datasets (Wang *et al.*, 2019; Liu *et al.*, 2020) prevents a quantitative correlation between these depositional features and the observed percolation behavior. This limitation highlights the need for future studies to integrate detailed facies analysis with petrophysical measurements to better constrain the sedimentological controls on pore network structure in tight rocks.

3.1.5 Permeability and porosity relationship

Despite the apparent relationship between porosity and permeability, this correlation is often circumstantial, as a single porosity value may correspond to permeability values spanning two to four orders of magnitude (Comiski *et al.*, 2007; Yokoyama and Takeuchi, 2009). The equivalence problem in petrophysical characterization, poses a significant challenge when attempting to estimate permeability solely based on porosity measurements. Figure 5a illustrates this phenomenon by plotting the porosity and permeability values of all samples used in this study, with the highlighted elliptical region demonstrating how rocks with

similar porosity values can exhibit vastly different permeability values. Conversely, Figure 4b presents the MICP curves and PTSD of three distinct rock samples (Sh4, Ca1, and Ts3) that possess remarkably similar permeability values (0.313 mD, 0.384 mD, and 0.467 mD, respectively), yet despite their comparable permeabilities, these samples display markedly different PTSD patterns corresponding to their varying porosity values. This dual observation, where similar porosities yield different permeabilities and similar permeabilities occur with different porosities, underscores that permeability values do not necessarily correlate with either porosity or PTSD patterns, highlighting the complex and non-unique relationship between these fundamental petrophysical properties in tight rocks.

3.2. Multilinear regression analysis of permeability, pore-throat radius, and evaluation of Poiseuille models

While the permeability-porosity relationship remains ambiguous, multiple studies have documented significant correlations between permeability and characteristic pore-throat radius (Comisky, 2007; Noorudin *et al.*, 2013). However, considerable uncertainty remains regarding which specific radius most effectively predicts permeability across different types of tight rock. To address this question, multiple characteristic radii were estimated from MICP curves, and a multilinear regression analysis was performed to identify the three radii with the strongest correlations for each rock type, using R^2 and RMSE as statistical performance metrics.

Poiseuille models were evaluated to estimate permeability in porous media. This analysis also examines the incorporating of transport porosity to assess the predictive capability of the models. This approach allows a physically representative characterization of the percolation in different pore networks.

The following subsections present the analysis of permeability-radius relationships and the Poiseuille models that aim to evaluate the sensitivity of permeability to porosity and transport porosity.

3.2.1 Tight sandstones

Figure 6 presents the analysis of permeability-radius relationships and Poiseuille-type models for tight sandstones. The multilinear regression analysis identified three characteristic radii with the strongest correlation to permeability in these samples. Consistently exhibit values exceeding 0.9, indicating that these radii capture 90% or more of the permeability variance. The radius that most effectively characterizes permeability in these samples is R_C, with an R^2 of 0.95, as is illustrated in Figure 6a; the remaining residual variance likely relates to additional factors such as tortuosity. Figure 6b and 6c shows the following characteristic radii from 20 to 25% of saturation, these predictive radii correspond to mercury saturations ranging from 20% to 27.5%, specifically between r_{20} and the average saturation of R_C. This range represents the critical fraction of the pore network required to achieve percolation in the tight sandstone used in this study. However, some samples with the

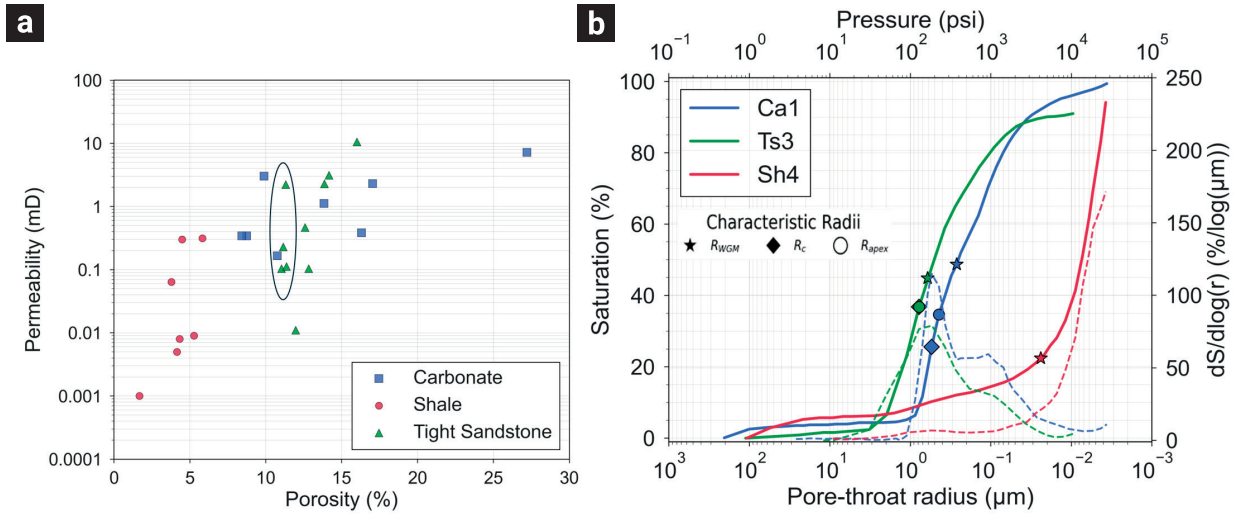

Figure 5. Permeability-porosity relationship in tight rocks. a) Cross-plot of porosity versus permeability values for all samples, highlighting regions where similar porosity values correspond to varying permeability measurements; b) Comparison of MICP curves and PTSD profiles for three rocks distinct samples (Sh4, Ca1, and Ts3) with similar permeability values (0.313-0.467 mD), demonstrating that rocks with comparable permeability can exhibit fundamentally different pore networks.

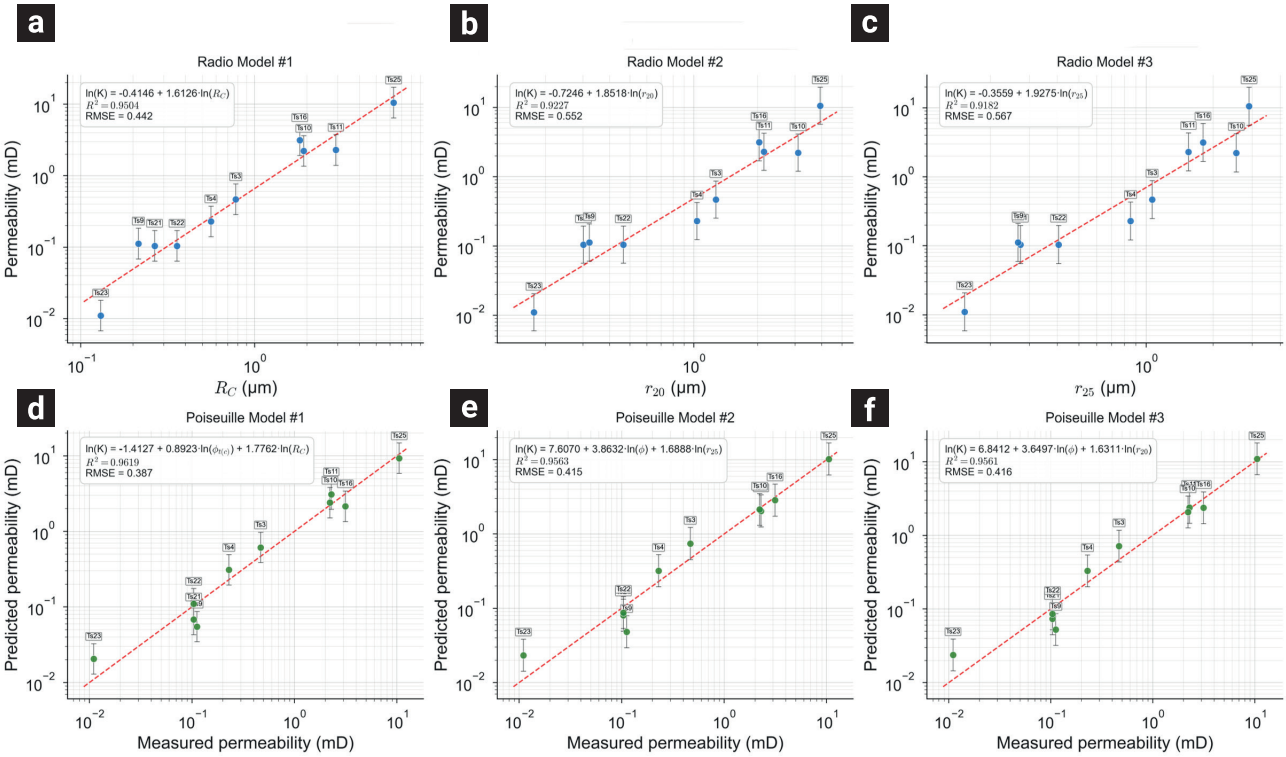

Figure 6. Correlation between permeability and characteristic pore-throat radius and evaluation of Poiseuille-type models for tight sandstones. (a-c) show the three strongest correlations with different characteristic radii; (d-f) present the corresponding Poiseuille model evaluations

highest permeability values can percolate at saturations below the range mentioned above.

Additionally, the Poiseuille models for tight sandstones demonstrate strong correlations with measured permeability values. Incorporating transport porosity into the model based on R_C yielded the highest predictive performance, achieving an R^2 value of 0.96, as shown in Figure 6d. This was followed closely by models utilizing r_{25} and r_{20}, which exhibited similar coefficients of determination, as illustrated in Figures 6e and 6f. Notably, while including porosity significantly enhanced the predictive capability of the r_{25} and r_{20} models, the single-parameter model based solely on R_C already achieved a remarkable R^2 of 0.95. The subsequent incorporation of transport porosity into the R_C model resulted in a slight but statistically significant improvement in predictive accuracy.

3.2.2 Carbonates

Figure 7 illustrates the analysis of permeability-radius relationships and Poiseuille-type models for carbonate samples. The multilinear regression analysis revealed three distinctive characteristic radii that most strongly correlate with permeability. Figure 7a and 7b show that the radius r_{70} and r_{65} demonstrate the highest R^2 values, with r_{70} showing marginally superior performance. Figure 7c shows that r_{60} also exhibits considerable predictive capacity. These influential radii correspond to saturation levels between 60% and 70%, significantly higher than in sandstones. This reflects the more complex pore network of carbonates and indicates the greater saturation required to establish effective percolation pathways.

The Poiseuille models for carbonates exhibit only marginal improvements in R^2 compared to their corresponding radii models. In particular, the models incorporating r_{70} and r_{65}, as illustrated in Figures 7d and 7e, show minimal enhancement when porosity is added. This indicates that these carbonate samples demonstrate stronger sensitivity to specific pore-throat radii than to porosity measurements. Conversely, the model incorporating r_{60} shows more substantial improvement when expanded into a complete Poiseuille formulation, as demonstrated in Figure 7f. Notably, these carbonate samples display limited sensitivity not only to porosity but also to transport porosity.

3.2.3 Shales

Figure 8 presents the analysis of permeability-radius relationships and Poiseuille-type models for shale samples. Figure 8a and

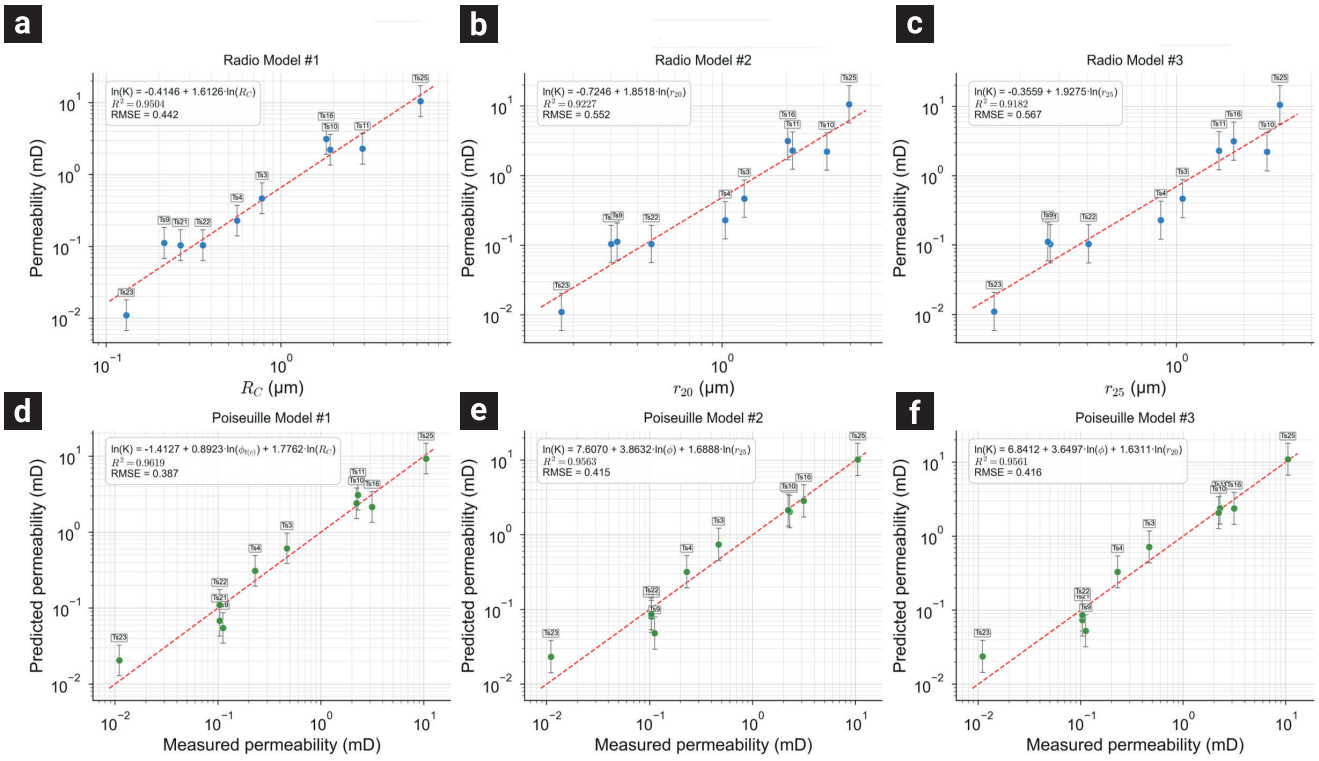

Figure 7. Correlation between permeability and characteristic pore-throat radius and evaluation of Poiseuille-type models for Carbonates. (a-c) show the three strongest correlations with different characteristic radii; (d-f) present the corresponding Poiseuille model evaluations.

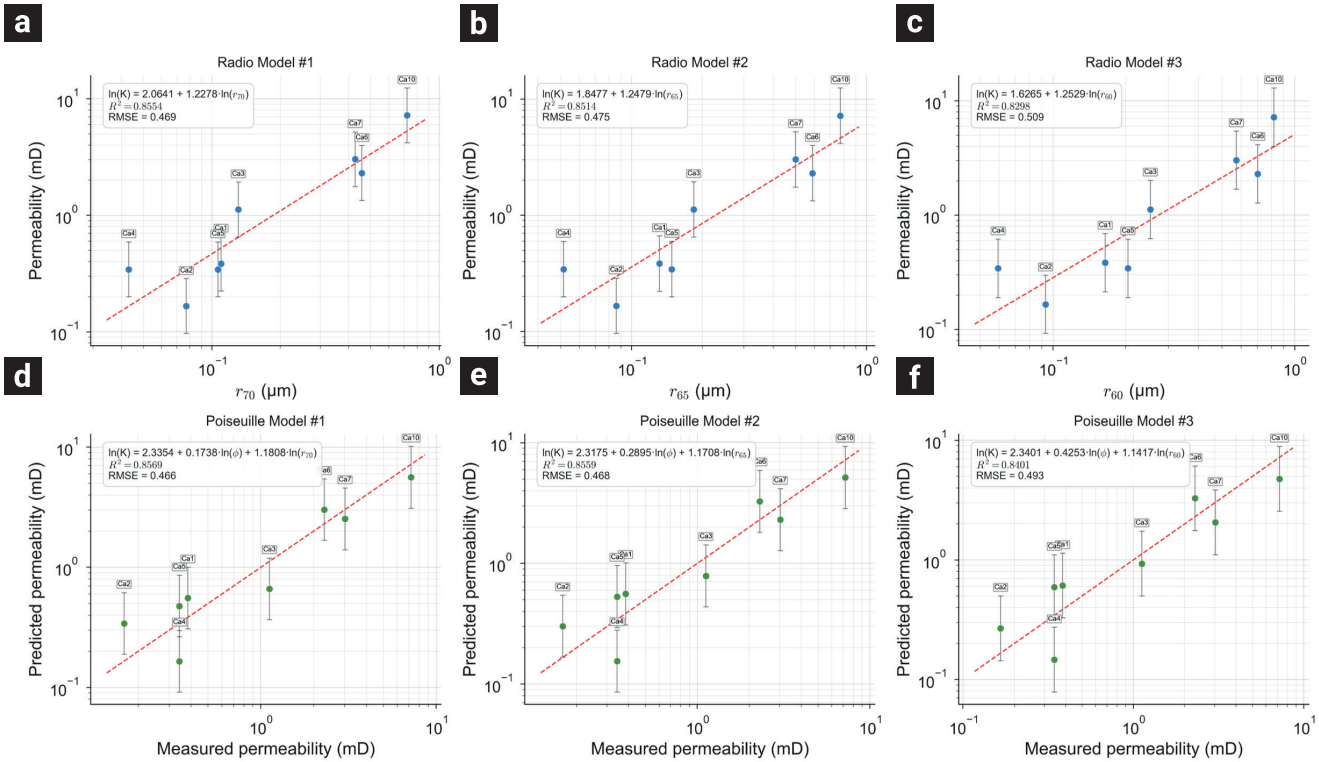

Figure 8. Correlation between permeability and characteristic pore-throat radius and evaluation of Poiseuille-type models for Shales. (a-c) show the three strongest correlations with different characteristic radii; (d-f) present the corresponding Poiseuille model evaluations

8b show r_{10} with an R^2 of 0.76 and R_{WGM} with 0.72, representing the most predictive radii, and Figure 8c shows a poor correlation with r_5. These models retain higher residual variance compared to the other rocks. This unexplained variance may be attributed to tortuosity effects, physicochemical processes specific to shales, contributions from other radii or other structural effects of the pore network, suggesting that modifications to the standard Poiseuille model could improve permeability predictions for these ultra-tight rocks. The critical saturation range for percolation in shales spans from 5% to 27.4%, corresponding to the larger pore-throats, despite the PTSD indicating that this size range is less prominent than the nanometer-scale pores that dominate these formations.

The Poiseuille models for shales maintain moderate predictive performance, with all R^2 values remaining below 0.8. Incorporating porosity into the r_{10} model yields only marginal improvement, as illustrated in Figure 8d. In contrast, the Poiseuille model incorporating r_5 substantially enhances in predictive capability, with R^2 increasing significantly from 0.66 to 0.76 when porosity is included, as shown in Figure 8e. Similarly, the model based on R_{WGM} also shows improvement by adding porosity. However, its overall performance remains slightly lower than the r_5 model, as depicted in Figure 8f. These results suggest that shales exhibit an intermediate sensitivity to porosity, more pronounced than observed in carbonates but less influential than in tight sandstones. This intermediate behavior likely reflects the distinctive nano-scale pore network of shale formations, where pore-throat dimensions and a fraction of the pore network contribute to the permeability.

3.2.4 Comparison with literature models

To evaluate the performance of the characteristic radii identified in this study, Poiseuille-type correlations were comparedwith established permeability prediction models from Table 1. Figure 9 presents these comparisons for each lithology, contrasting the proposed models (R_C for sandstones, r_{60} for carbonates, and r_{10} for shales) with models commonly used in literature. This analysis serves to assess whether systematically selected characteristic radii offer advantages over traditional approaches across different rock types

Figure 9a demonstrates that the R_C-based correlation achieves R^2= 0.96 for tight sandstones, outperforming the other tested literature models. While this high correlation derives from the same dataset and may not generalize perfectly to other samples, the primary objective was identifying the physically meaningful characteristic radius rather than developing a universal correlation. The Rezaee model shows the next best performance (R^2 = 0.81), likely because this low percentile radius partially captures flow-controlling elements in tight formations. The Pittman models using r_{25} and R_{apex} yield lower correlations (R^2 = 0.53 and 0.45), suggesting that while these radii may be representative for some systems, their associated empirical parameters fail to adequately capture the permeability variance in the samples presented in this work. For these tight sandstones with preserved intergranular connectivity, the percolation-based R_C provides the most physically representative characterization of permeability.

Figure 9b shows that the r_{70}-based correlation achieves R^2 = 0.86 for carbonates, the highest among all tested models. Among literature models, Ngo r_{20} performs best with R^2 = 0.55, followed by Rezaee r_{30} at R^2 = 0.49. These models using lower percentile radii (25-30%) cannot adequately represent carbonate's pore network complexity, where flow depends on narrow throats connecting isolated vugs and moldic pores. The saturation requirement of 60 to 70 percent indicates that mercury must invade multiple pore systems, including primary porosity as well as secondary dissolution pores, before achieving continuous pathways. Unlike models assuming dominant pore-throat radius, this approach captures the cumulative saturation needed to interconnect heterogeneous carbonate pore networks. Figure 9c illustrates the challenge of predicting shale permeability, where the proposed r_{10}-based correlation (R^2 = 0.77) stands in stark contrast to the poor predictions of all tested literature models (negative R^2 values). The Dastidar model's poor performance (R^2 = -9.80), despite using weighted geometric mean designed for tight rocks, indicates fundamental incompatibility with nanoporous shale systems. The Rezaee r_{10} model (R^2 = -3.82), successful in tight sandstones, fails when applied to shales, demonstrating that models cannot transfer between rock types without accounting for distinct pore network configurations, although the same radius is applied. On the other hand, the Vafaie model's (R^2 = -4.18) despite being developed specifically for shales, suggesting limited generalizability across different basins. While r_{10} approach shows modest performance compared to other lithologies, it represents the only functional predictive method among those tested. This validates that low percentile radii capturing the narrowest flow-controlling elements are essential for shale characterization, though results underscore the need for new theoretical frameworks tailored to ultra-tight formations.

3.3. Comparative analysis of percolation thresholds across tight rock types

The published models summarized in Table 1 identify different characteristic radii correlating with permeability. While these correlations may be statistically significant, the methodology presented in this work emphasizes the identification of the radius that physically represents the critical saturation

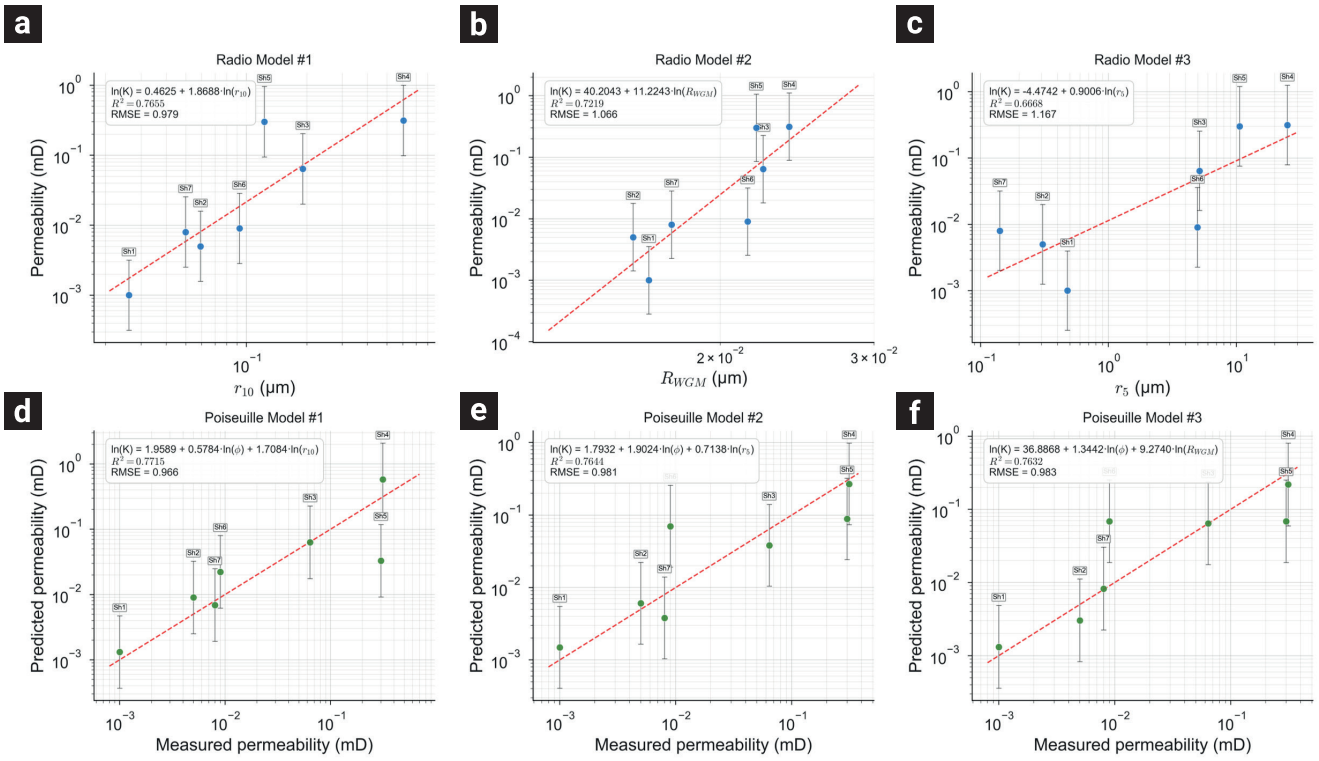

Figure 9. Comparison of measured versus predicted permeability for (a) tight sandstones, (b) carbonates, and (c) shales. Red circles represent Poiseuille-type correlations using the identified characteristic radii (R_C, r_{70}, r_{10} and respectively), while other symbols show literature models specific to each lithology. The dashed line indicates perfect 1:1 prediction. R^2 values quantify model performance, with negative values indicating predictions worse than using mean permeability. The systematic selection of characteristic radii based on percolation behavior provides functional predictions across all lithologies, contrasting with the failure of established models for shales.

threshold at which percolation is achieved in different types of tight rock. Published models indicate saturation ranges between 10% and 35% for optimal characteristic radius for tight sandstones (Dastidar *et al.*, 2007; Rezaee *et al.*, 2012); however, the results reveal a narrower, range of 20% to 27.5%. This range reflects that even after substantial porosity reduction, lacustrine turbidite sandstones maintain sufficient pore-throat connectivity to enable percolation at moderate saturations. The preserved intergranular connectivity suggests that the pore networks of these tight sandstones are particularly sensitive to the R_C concept, which captures the percolation threshold where continuous flow paths first establish. Notably, some samples exhibit percolation at lower saturation percentages, such as Ts25, which coincides with higher permeability values and pore-throat radii in the micrometer scale as shown in Figure 10.

Previous studies of carbonates suggest saturation ranges from 20% to 50% for characteristic radius (Rezaee *et al.*, (2006); Ngo *et al.*, (2018)), whereas the samples presented demonstrate significantly higher values ranging from 53% to 70%. This discrepancy likely reflects the complex pore networks inherited from diverse carbonated ramp environments and their subsequent diagenetic evolution, where heterogeneous pore networks require greater mercury saturation to establish percolation pathways compared to carbonates with simpler, more connected pore networks. Importantly, the characteristic radii r_{60}-r_{70} represent pore-throat dimensions that are orders of magnitude smaller than the vugs and moldic pores they connect, indicating that despite the presence of large secondary pores, permeability is controlled by the narrow throats linking these isolated pore bodies, which explains why porosity adds minimal predictive value to Poiseuille models in these samples, as Liu *et al.* (2020) suggested, incorporating a more representative characteristic radius better captures the complex pore network of these carbonates.

For shales, published literature reports a characteristic saturation of approximately 55% (Vafaie *et al.*, 2021), which contrasts with the observed range of 5% to 27.5%. This lower range provides validation for Pittman's (1992) observation that samples with essentially straight MICP curves, in which a dominant modal pore size is absent, would have their percolation-controlling elements below 10% saturation, precisely where the optimal correlations with r_5-r_{10} were identified. This behavior likely reflects the fine-grained nature of lacustrine shales deposited

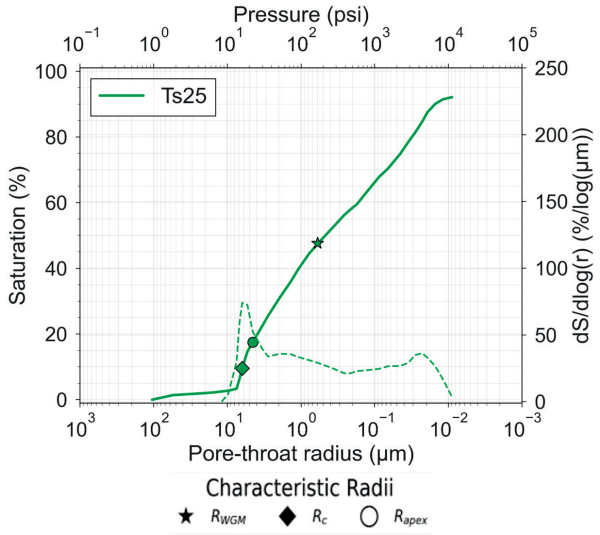

Figure 10. Analysis of sample Ts25 shows R_C and R_{apex} corresponding to saturation levels below 20%, indicating an early percolation threshold.

in stratified, anoxic settings, where clay-dominated fabrics and heterogeneous organic matter distribution create nanoscale pore networks lacking well-defined modal sizes.

While radii and Poiseuille models simplify the complex connectivity of pore networks to a single characteristic radius, the developed analysis demonstrates that these approaches can provide practical estimations of permeability, identify the characteristic radius that represents the percolation thresholds for each type of tight rock, offering rock-specific solutions rather than attempting universal correlations.

For rocks with particularly complex pore networks, such as shales, complementary analytical techniques, like N_2 adsorption isotherms, could be integrated to characterize the domains beyond the resolution limits of MICP. Such multi-technique approaches could establish more sophisticated models that better capture the multiscale nature of these intricate pore systems, potentially enhancing permeability prediction accuracy. As Vafaie *et al.*, (2021) noted, developing a truly universal permeability model remains an active and challenging area of research; this work contributes to this ongoing effort by demonstrating the importance of rock-specific approaches that recognize the fundamental differences in pore networks.

4. Conclusions

Through the novel method introduced in this work, analysis of MICP data from tight rocks identified specific characteristic radii that influence permeability in each lithology. These findings give reservoir geologists, petrophysicists, and petroleum engineers practical tools for estimating permeability in unconventional reservoirs, CO2 storage projects, and enhanced recovery operations, where routine MICP measurements serve as a cost-effective alternative to specialized permeability tests.

Tight sandstones were controlled by the critical radius (R_C) at 27.5% average saturation. The observed sensitivity to transport porosity in Poiseuille models indicates that both pore-throat radius and the volume of interconnected pores contribute to permeability, characteristic of rocks with preserved intergranular porosity where flow paths remain relatively accessible.

Carbonates required higher percentile radii (r_{60} to r_{70}) to achieve percolation. Their minimal porosity sensitivity indicates that permeability is controlled primarily by the narrow throats connecting larger pore bodies, typical of rocks with secondary porosity where vugs and molds are linked by constricted passages.

Shales correlated with the lowest percentile radii (r_5 to r_{10}) the control by these smallest radii reflects the dominance of nanoscale pore-throats (26-191 nm) in determining permeability, despite their limited abundance.

Despite being semi-empirical approximations, Poiseuille models provide practical permeability estimations when direct measurements are unavailable. The models developed captured 76-96% permeability variance across different lithologies by incorporating rock-specific characteristic radii.

These findings demonstrate that permeability prediction in tight rocks requires lithology-specific approaches. However, establishing definitive links between sedimentological controls and percolation behavior necessitates future studies that integrate detailed geological characterization with petrophysical measurements. Such integrated approaches are essential for reservoir characterization and CO2 storage assessment in tight formations.

5. Acknowledge

The authors, Franco-Villegas and Nieto-Rivero, thank the SECIHTI (Secretaria de Ciencia, Humanidades, Tecnología e Innovación) for its financial support and the Graduate Program of the IMP for its support. All authors thank the Instituto Mexicano del Petróleo (IMP) for permission to publish this work.

6. Declarations

The authors declare that they have no known competing financial interests or personal relationships that could have appeared to influence the work reported in this paper.

7. Nomenclature

k, permeability, (mD)
ϕ, porosity (fraction)
ϕ_t, transport porosity (fraction)
r, capillary radius (μm)
P_C, capillary pressure (psi)
γ, surface tension (N/m)
θ, contact angle (°)
r_n, n-th percentil radius (μm)
R_C, Critical radius (μm)
R_{WGM}, Weighted geometrical mean radius (μm)
R_{apex}, Apex radius (μm)
R_i, i-th radius (μm)
w_i, contribution weight (adim)
a_i, incremental saturation (fraction)
a_T, total incremental saturation (fraction)
$S_{\%}$, saturation (fraction)
$_C$, geometrical constant (adim)
R^2, coefficient determination (adim)
$RMSE$, root mean square error (adim)
Q, volumetric flow rate (m^3/s)
N, total number of capillaries (adim)
ΔP, pressure drop across capillary (Pa)
μ, dynamic viscosity of fluid (Pa*s)
L, capillary length (m)
A, Cross sectional area (m^2)

8. References

Al-Aasm, I. S., Ghazban, F., & Ranjbaran, M. (2009). Dolomitization and related fluid evolution in the oligocene–miocene asmari formation, gachsaran area, sw Iran: petrographic and isotopic evidence. Journal of Petroleum Geology, 32(3), 287-304. doi: **https://doi.org/10.1111/j.1747-5457.2009.00449.x**

Amann-Hildenbrand, A., Bertier, P., Busch, A., & Krooss, B. M. (2013). Experimental investigation of the sealing capacity of generic clay-rich caprocks. International Journal of Greenhouse Gas Control, 19, 620-641. doi: **https://doi.org/10.1016/j.ijggc.2013.01.040**

Aqrawi, A. A. M., Keramati, M., Ehrenberg, S. N., Pickard, N., Moallemi, A., Svånå, T., Darke, G., Dickson, J. A. D., & Oxtoby, N. H. (2006). The origin of dolomite in the asmari formation (oligocene-lower miocene), dezful embayment, sw Iran. Journal of Petroleum Geology, 29(4), 381-402. doi: **https://doi.org/10.1111/j.1747-5457.2006.00381.x**

Bear, J. (2018). *Modeling Phenomena of Flow and Transport in Porous Media* (Vol. 31). Springer International Publishing. doi: **https://doi.org/10.1007/978-3-319-72826-1**

Bernabé, Y., Li, M., & Maineult, A. (2010). Permeability and pore connectivity: A new model based on network simulations. *Journal of Geophysical Research: Solid Earth, 115*(B10), 2010JB007444. doi: **https://doi.org/10.1029/2010JB007444**

Boak, J., & Kleinberg, R. (2020). Shale Gas, Tight Oil, Shale Oil and Hydraulic Fracturing. In Trevor M. Letcher (Ed.) *Future Energy* (pp. 67-95). Elsevier. doi: **https://doi.org/10.1016/B978-0-08-102886-5.00004-9**

Comisky, J. T., Newsham, K. E., Rushing, J. A., & Blasingame, T. A. (2007). A Comparative Study of Capillary-Pressure-Based Empirical Models for Estimating Absolute Permeability in Tight Gas Sands. *SPE Annual Technical Conference and Exhibition,* SPE-110050-MS. doi: **https://doi.org/10.2118/110050-MS**

Dastidar, R., Sondergeld, C. H., & Rai, C. S. (2007). An Improved Empirical Permeability Estimator From Mercury Injection For Tight Clastic Rocks. *Petrophysics - The SPWLA Journal, 48*(03).

Er, C., Li, Y., Zhao, J., Wang, R., Bai, Z., & Han, Q. (2016). Pore formation and occurrence in the organic-rich shales of the Triassic Chang-7 Member, Yanchang Formation, Ordos Basin, China. Journal of Natural Gas Geoscience, 1(6), 435-444. doi: **https://doi.org/10.1016/j.jnggs.2016.11.013**

Feng, Z., & Graham, S. A. (2024). The Songliao basin, China. In Domenico Chiarella, Nicola Scarselli and Jürgen Adam (Eds.) *Regional Geology and Tectonics* (pp. 121-145). Elsevier. doi: **https://doi.org/10.1016/B978-0-444-64136-6.00003-8**

Fleury, M., & Brosse, E. (2018). Transport in Tight Rocks. En S. Vialle, J. Ajo-Franklin, & J. W. Carey (Eds.), *Geophysical Monograph Series* (1a ed., pp. 31-43). Wiley. doi: **https://doi.org/10.1002/9781119118657.ch2**

Gao, Z., & Hu, Q. (2013). Estimating permeability using median pore-throat radius obtained from mercury intrusion porosimetry. *Journal of Geophysics and Engineering*, 10(2), 025014. doi: **https://doi.org/10.1088/1742-2132/10/2/025014**

Giesche, H. (2006). Mercury Porosimetry: A General (Practical) Overview. *Particle & Particle Systems Characterization*, 23(1), 9-19. doi: **https://doi.org/10.1002/ppsc.200601009**

Hildenbrand, A., Schlömer, S., & Krooss, B. M. (2002). Gas breakthrough experiments on fine-grained sedimentary rocks. *Geofluids*, 2(1), 3-23. doi: **https://doi.org/10.1046/j.1468-8123.2002.00031.x**

Hu, F., Meng, Q., & Liu, Z. (2021). Mineralogy and Element Geochemistry of Oil Shales in the Lower Cretaceous Qingshankou Formation of the Southern Songliao Basin, Northeast China: Implications of Provenance, Tectonic Setting, and Paleoenvironment. ACS Earth and Space Chemistry, 5(2), 365-380. doi: **https://doi.org/10.1021/acsearthspacechem.0c00336**

Huet, C. C., Rushing, J. A., Newsham, K. E., & Blasingame, T. A. (noviembre, 2005). A Modified Purcell/Burdine Model for Estimating Absolute Permeability from Mercury-Injection Capillary Pressure Data. All Days. [Presentación de paper]. International Petroleum Technology Conference, Doha, Qatar. doi: **https://doi.org/10.2523/iptc-10994-ms**

Hunt, A. G. (2001). Applications of percolation theory to porous media with distributed local conductances. *Advances in Water Resources, 24*(3-4), 279-307. doi: **https://doi.org/10.1016/S0309-1708(00)00058-0**

Katz, A. J., & Thompson, A. H. (1986). Quantitative prediction of permeability in porous rock. *Physical Review B, 34*(11), 8179-8181. doi: https://doi.org/10.1103/PhysRevB.34.8179

Katz, A. J., & Thompson, A. H. (1987). Prediction of rock electrical conductivity from mercury injection measurements. *Journal of Geophysical Research: Solid Earth, 92*(B1), 599-607. doi: **https://doi.org/10.1029/JB092iB01p00599**

Kolodzie, S. (1980). Analysis of Pore Throat Size and Use of the Waxman-Smits Equation to Determine OOIP in Spindle Field, Colorado. [Presentación de paper] *SPE Annual Technical Conference and Exhibition*, SPE-9382-MS. doi: **https://doi.org/10.2118/9382-MS**

León Y León, C. A. (1998). New perspectives in mercury porosimetry. Advances in Colloid and Interface Science, 76-77, 341-372. doi: **https://doi.org/10.1016/s0001-8686(98)00052-9**

Liu, K., Mirzaei-Paiaman, A., Liu, B., & Ostadhassan, M. (2020). A new model to estimate permeability using mercury injection capillary pressure data: Application to carbonate and shale samples. *Journal of Natural Gas Science and Engineering, 84*, 103691. doi: **https://doi.org/10.1016/j.jngse.2020.103691**

Liu, K., & Ostadhassan, M. (2019). The impact of pore size distribution data presentation format on pore structure interpretation of shales. *Advances in Geo-Energy Research, 3*(2), 187-197. doi: **https://doi.org/10.26804/ager.2019.02.08**

Mohaghegh, S., Arefi, R., Bilgesu, I., Ameri, S., & Rose, D. (1995). Design and Development of An Artificial Neural Network for Estimation of Formation Permeability. *SPE Computer Applications*, 7(06), 151-154. doi: **https://doi.org/10.2118/28237-PA**

Ngo, V. T., Lu, V. D., & Le, V. M. (2018). A comparison of permeability prediction methods using core analysis data for sandstone and carbonate reservoirs. *Geomechanics and Geophysics for Geo-Energy and Geo-Resources, 4*(2), 129-139. doi: **https://doi.org/10.1007/s40948-017-0078-y**

Ngo, V. T., Lu, V. D., Nguyen, M. H., Hoang, T. M., Nguyen, H. M., & Le, V. M. (2015). A Comparison of Permeability Prediction Methods Using Core Analysis Data. [Presentación de paper]. *SPE Reservoir Characterisation and Simulation Conference and Exhibition*, D011S001R003. doi: **https://doi.org/10.2118/175650-MS**

Nooruddin, H. A., Anifowose, F., & Abdulraheem, A. (2013). Applying Artificial Intelligence Techniques to Develop Permeability Predictive Models using Mercury Injection Capillary-Pressure Data. [Presentación de paper]. *SPE Saudi Arabia Section Technical Symposium and Exhibition*, SPE-168109-MS. doi: **https://doi.org/10.2118/168109-MS**

Ozotta, O., Ostadhassan, M., Liu, K., Liu, B., Kolawole, O., & Hadavimoghaddam, F. (2021). Reassessment of CO2 sequestration in tight reservoirs and associated formations. *Journal of Petroleum Science and Engineering, 206*, 109071. doi: **https://doi.org/10.1016/j.petrol.2021.109071**

Pickup, G. E., Ringrose, P. S., Jensen, J. L., & Sorbie, K. S. (1994). Permeability tensors for sedimentary structures. *Mathematical Geology, 26*(2), 227-250. doi: **https://doi.org/10.1007/BF02082765**

Pittman, E. D. (1992). Relationship of porosity and permeability to various parameters derived from mercury injection-capillary pressure curves for sandstone. *AAPG Bulletin (American Association of Petroleum Geologists); (United States), 76(2).* **https://www.osti.gov/biblio/5597475**

Qin, Y., Yao, S., Xiao, H., Cao, J., Hu, W., Sun, L., Tao, K., & Liu, X. (2021). Pore structure and connectivity of tight sandstone reservoirs in petroleum basins: A review and application of new methodologies to the Late Triassic Ordos Basin, China. Marine and Petroleum Geology, 129, 105084. doi: **https://doi.org/10.1016/j.marpetgeo.2021.105084**

Rashid, F., Glover, P. W. J., Lorinczi, P., Hussein, D., Collier, R., & Lawrence, J. (2015). Permeability prediction in tight carbonate rocks using capillary pressure measurements. *Marine and Petroleum Geology, 68(A)*, 536-550. doi: **https://doi.org/10.1016/j.marpetgeo.2015.10.005**

Rezaee, M. R., Jafari, A., & Kazemzadeh, E. (2006). Relationships between permeability, porosity and pore throat size in carbonate rocks using regression analysis and neural networks. *Journal of Geophysics and Engineering, 3*(4), 370-376. doi: **https://doi.org/10.1088/1742-2132/3/4/008**

Rezaee, R., Saeedi, A., & Clennell, B. (2012). Tight gas sands permeability estimation from mercury injection capillary pressure and nuclear magnetic resonance data. *Journal of Petroleum Science and Engineering, 88-89*, 92-99. doi: **https://doi.org/10.1016/j.petrol.2011.12.014**

Sadeqi, H., Aleali, M., Kadkhodaie, A., & Arian, M. (2025). Facies distribution, sequence stratigraphy, and reservoir quality of the Oligo-Miocene carbonate sequences (Asmari formation) in the Dezful embayment, SW Iran. Journal of Petroleum Exploration and Production Technology, 15(1), 2. doi: **https://doi.org/10.1007/s13202-024-01892-7**

Sahimi, M. (2021). Percolation Phase Transition. En M. Sahimi & A. G. Hunt (Eds.), *Complex Media and Percolation Theory* (pp. 1-9). Springer US. doi: **https://doi.org/10.1007/978-1-0716-1457-0_387**

Salazar, M. O., & Villa, J. R. (2007). Permeability Upscaling Techniques for Reservoir Simulation. [Presentación de paper]. *Latin American & Caribbean Petroleum Engineering Conference*, SPE-106679-MS. doi: **https://doi.org/10.2118/106679-MS**

Seyrafian, A., Vaziri-Moghaddam, H., Arzani, N., & Taheri, A. (2011). Facies analysis of the Asmari Formation in central and north-central Zagros basin, southwest Iran: Biostratigraphy, paleoecology and diagenesis. Revista Mexicana de Ciencias Geológicas, 28(3), 439-458. **https://rmcg.geociencias.unam.mx/index.php/rmcg/article/view/184**

Sun, M., Zhang, L., Hu, Q., Pan, Z., Yu, B., Sun, L., Bai, L., Fu, H., Zhang, Y., Zhang, C., & Cheng, G. (2020). Multiscale connectivity characterization of marine shales in southern China by fluid intrusion, small-angle neutron scattering (SANS), and FIB-SEM. *Marine and Petroleum Geology*, 112, 104101. doi: **https://doi.org/10.1016/j.marpetgeo.2019.104101**

Swanson, B. F. (1981). Simple correlation between permeabilities and mercury capillary pressures. *Journal of Petroleum Technololgy*, 33(12), 2498–2504. doi: **https://doi.org/10.2118/8234-PA**

Vafaie, A., Kivi, I. R., Moallemi, S. A., & Habibnia, B. (2021). Permeability prediction in tight gas reservoirs based on pore structure characteristics: A case study from South Western Iran. *Unconventional Resources, 1,* 9-17. doi: **https://doi.org/10.1016/j.uncres.2021.08.001**

Vaziri-Moghaddam, H., Kimiagari, M., & Taheri, A. (2006). Depositional environment and sequence stratigraphy of the Oligo-Miocene Asmari Formation in SW Iran. Facies, 52(1), 41-51. doi: **https://doi.org/10.1007/s10347-005-0018-0**

Wang, F., Yang, K., You, J., & Lei, X. (2019). Analysis of pore size distribution and fractal dimension in tight sandstone with mercury intrusion porosimetry. *Results in Physics, 13*, 102283. doi: **https://doi.org/10.1016/j.rinp.2019.102283**

Wang, S., Javadpour, F., & Feng, Q. (2016). Confinement Correction to Mercury Intrusion Capillary Pressure of Shale Nanopores. *Scientific Reports*, 6(1), 20160. doi: **https://doi.org/10.1038/srep20160**

Washburn, E. W. (1921). The Dynamics of Capillary Flow. *Physical Review Journal Archive*, 17(3), 273-283. doi: **https://doi.org/10.1103/PhysRev.17.273**

Webb, P. A., (2001). An Introduction to the Physical Characterization of Materials by Mercury Intrusion Porosimetry with Emphasis on Reduction and Presentation of Experimental Data. Micromeritics Instrument Corp., Norcross, Georgia.

Yang, H., & Deng, X. (2013). Deposition of Yanchang Formation deep-water sandstone under the control of tectonic events in the Ordos Basin. *Petroleum Exploration and Development, 40*(5), 549-557. doi: **https://doi.org/10.1016/S1876-3804(13)60072-5**

Yokoyama, T., & Takeuchi, S. (2009). Porosimetry of vesicular volcanic products by a water-expulsion method and the relationship of pore characteristics to permeability. *Journal of Geophysical Research: Solid Earth, 114*(B2), 2008JB005758. doi: **https://doi.org/10.1029/2008JB005758**

Zhang, P., Misch, D., Hu, F., Kostoglou, N., Sachsenhofer, R. F., Liu, Z., Meng, Q., & Bechtel, A. (2021). Porosity evolution in organic matter-rich shales (Qingshankou Fm.; Songliao Basin, NE China): Implications for shale oil retention. Marine and Petroleum Geology, 130, 105139. doi: **https://doi.org/10.1016/j.marpetgeo.2021.105139**

Zhao, X., Sun, M., Ukaomah, C. F., Ostadhassan, M., Cui, Z., Liu, B., & Pan, Z. (2023). Pore connectivity and microfracture characteristics of Longmaxi shale in the Fuling gas field: Insights from mercury intrusion capillary pressure analysis. *Gas Science and Engineering, 119*(A), 205134. doi: **https://doi.org/10.1016/j.jgsce.2023.205134**

Zhang, X.-S., Wang, H.-J., Ma, F., Sun, X.-C., Zhang, Y., & Song, Z.-H. (2016). Classification and characteristics of tight oil plays. *Petroleum Science, 13*(1), 18-33. doi: **https://doi.org/10.1007/s12182-015-0075-0**